Crystal Structure of the *Caenorhabditis elegans* Apoptosome Reveals an Octameric Assembly of CED-4

Shiqian Qi,[1,6] Yuxuan Pang,[2,6] Qi Hu,[2,7] Qun Liu,[3,7] Hua Li,[4] Yulian Zhou,[1] Tianxi He,[5] Qionglin Liang,[5] Yexing Liu,[1] Xiaoqiu Yuan,[2] Guoan Luo,[5] Huilin Li,[4] Jiawei Wang,[2] Nieng Yan,[2,*] and Yigong Shi[1,*]

[1]Ministry of Education Protein Science Laboratory
[2]State Key Laboratory of Biomembrane, Center for Structural Biology
School of Life Sciences and School of Medicine, Tsinghua University, Beijing 100084, China
[3]New York Structural Biology Center
[4]Biology Department
Brookhaven National Laboratory, Upton, NY 11973, USA
[5]Department of Chemistry, Tsinghua University, Beijing 100084, China
[6]These authors contributed equally to this work
[7]These authors contributed equally to this work
*Correspondence: nyan@tsinghua.edu.cn (N.Y.), shi-lab@tsinghua.edu.cn (Y.S.)

SUMMARY

The CED-4 homo-oligomer or apoptosome is required for initiation of programmed cell death in *Caenorhabditis elegans* by facilitating autocatalytic activation of the CED-3 caspase zymogen. How the CED-4 apoptosome assembles and activates CED-3 remains enigmatic. Here we report the crystal structure of the complete CED-4 apoptosome and show that it consists of eight CED-4 molecules, organized as a tetramer of an asymmetric dimer via a previously unreported interface among AAA+ ATPases. These eight CED-4 molecules form a funnel-shaped structure. The mature CED-3 protease is monomeric in solution and forms an active holoenzyme with the CED-4 apoptosome, within which the protease activity of CED-3 is markedly stimulated. Unexpectedly, the octameric CED-4 apoptosome appears to bind only two, not eight, molecules of mature CED-3. The structure of the CED-4 apoptosome reveals shared principles for the NB-ARC family of AAA+ ATPases and suggests a mechanism for the activation of CED-3.

INTRODUCTION

Programmed cell death (PCD), also known as apoptosis, is essential to metazoan development and tissue homeostasis (Danial and Korsmeyer, 2004; Horvitz, 2003). The biochemical pathway for the initiation of apoptosis is conserved across species, culminating in the activation of cell-killing proteases known as caspases (Yan and Shi, 2005). In *Caenorhabditis elegans* (*C. elegans*), PCD is carried out by the CED-3 caspase.

Similar to all known caspases, CED-3 is synthesized as an inactive zymogen in cells and its maturation involves autocatalytic cleavages. Autoactivation of CED-3 strictly depends on the adaptor protein CED-4. In response to cell death stimuli, CED-4 is released from an inactive complex containing an asymmetric homodimer of CED-4 and one molecule of the anti-death protein CED-9 (Yan et al., 2004, 2005). The freed CED-4 protein further oligomerizes to assemble into a higher-order homo-oligomer, hereafter referred to as the CED-4 apoptosome, which recruits CED-3 zymogen and facilitates its autocatalytic activation (Yan et al., 2006b; Yang et al., 1998a). Preliminary analysis by electron microscopy (EM) revealed that the CED-4 apoptosome exhibited a four-fold symmetry, which was thought to correspond to a tetramer (Yan et al., 2005).

The mammalian protein Apaf-1 is a CED-4 homolog (Zou et al., 1997). Under homeostatic conditions, Apaf-1 exists in an autoinhibited state (Li et al., 1997; Riedl et al., 2005). In response to apoptotic stimuli, Apaf-1 binds to cytochrome *c* and undergoes a nucleotide exchange process, which drives the formation of an oligomeric apoptosome (Bao et al., 2007; Kim et al., 2005; Li et al., 1997). The Apaf-1 apoptosome recruits caspase-9, a CED-3 homolog, and mediates its autocatalytic activation. In the absence of Apaf-1, caspase-9 can be activated through forced dimerization (Chao et al., 2005; Renatus et al., 2001; Yin et al., 2006). However, how exactly the Apaf-1 apoptosome activates caspase-9 remains enigmatic (Shi, 2004), and a conclusive answer to this question may require detailed structural information of the Apaf-1 apoptosome bound to caspase-9. EM analysis revealed that the Apaf-1 apoptosome existed mainly as a disc-shaped homo-heptamer (Acehan et al., 2002; Yu et al., 2005). The fruit fly homolog of Apaf-1 was identified as Dark (Rodriguez et al., 1999), Hac-1, or Dapaf-1 (Kanuka et al., 1999; Zhou et al., 1999). Dark, known to form an octameric apoptosome (Yu et al., 2006), is responsible for the activation of the caspase Dronc, a homolog of CED-3 and caspase-9.

Assembly of apoptosomes is a central event in apoptosis (Bao and Shi, 2007). At present, structural information on the apoptosome is exclusively derived from EM-based investigation and computational modeling (Acehan et al., 2002; Diemand and Lupas, 2006; Yu et al., 2005, 2006). Due to low resolution of the EM studies and the hypothetical nature of modeling, the essential features of apoptosomes are yet to be elucidated. Consequently, mechanistic understanding on apoptosome assembly and function has been slow to emerge.

CED-4, Apaf-1, and Dark share a number of unique sequence features, including a caspase recruitment domain (CARD) at their N termini, followed by a nucleotide-binding α/β-fold, a small helical domain (helical domain 1, or HD1), a winged-helix domain (WHD), and helical domain 2 (HD2). These sequence features are similar to several other families of signaling proteins, such as the pathogen resistance proteins (R proteins) in plants (Belkhadir et al., 2004; Takken et al., 2006; van Ooijen et al., 2008). The R proteins are activated in response to pathogen invasion and trigger-localized PCD (known as hypersensitive response) (Martin et al., 2003). Collectively, these signaling proteins define a unique family known as NB-ARC (nucleotide-binding, Apaf-1, R proteins, and CED-4) (van der Biezen and Jones, 1998), which belong to the AAA$^+$ superfamily of ATPases (Lupas and Martin, 2002). The active form of the NB-ARC proteins is thought to be oligomeric. Despite vigorous efforts, there is no detailed structural information on any of the oligomeric NB-ARC proteins. Understanding the structure and function of the apoptosome may shed light on the NB-ARCs, particularly on the R proteins.

In this manuscript, we report the structure of the complete CED-4 apoptosome, revealing insights into apoptosome assembly that may be applicable to other apoptosomes. To elucidate the mechanisms of assembly and those involved in the activation of CED-3, we performed structure-guided biochemical analysis. The conclusions derived from this study may be helpful for mechanistic understanding of other NB-ARC proteins.

RESULTS

Overall Structure of the CED-4 Apoptosome

Using a published protocol (Yan et al., 2005), we generated a homogeneous CED-4 apoptosome and obtained several crystal forms. Unfortunately none of these crystals diffracted X-rays beyond 10 Å resolution, likely due to crystal packing imperfection caused by flexible surface loops. To remedy this problem, we subjected the CED-4 apoptosome to limited proteolysis, which removed a surface loop comprising residues 498–517 (Figure S1A available online). The resulting CED-4 apoptosome retained the same ability to facilitate autocatalytic activation of CED-3 as the undigested CED-4 (Figure S1B). We succeeded in the generation of diffraction-quality crystals for the proteolysed CED-4 apoptosome and determined its X-ray structure at 3.55 Å resolution (Table S1). Each asymmetric unit contains an asymmetric dimer of CED-4, and the CED-4 apoptosome is formed via a crystallographic four-fold symmetry.

The CED-4 apoptosome has a funnel-shaped architecture, with a height of ∼110 Å and a diameter of ∼170 Å (Figure 1, Figures S1C and S1D). The assembly contains eight molecules

of CED-4, arranged as a tetramer of an asymmetric dimer. Each CED-4 contains an ATP molecule and a Mg^{2+} ion, both buried in the assembly and inaccessible to water molecules (Figure 1A, Figure S1E). The eight CARDs form two staggered, tetrameric rings at the narrow end of the funnel-shaped complex, giving rise to an overall four-fold symmetry (Figure 1A). Four CARDs, one from each asymmetric CED-4 dimer, associate with each other to assemble into a closed, tetrameric ring; whereas the other four CARDs are interspersed by CARDs of the closed ring. In our previous EM-based study, this four-fold symmetry was thought to come from four molecules of CED-4 (Yan et al., 2005); however, fitting four molecules of CED-4 into the EM density still left a substantial portion of the electron density unoccupied. This conundrum is nicely resolved by revelation of the present crystal structure—the basic unit of the CED-4 apoptosome is an asymmetric dimer, rather than a single molecule, of CED-4.

The CED-4 apoptosome contains a cone-shaped, interior space that measures 50 Å in height and 36–90 Å in diameters (Figure 1B). This space, hereafter referred to as the "hutch," is large enough to accommodate a folded, globular protein with molecular weight of 60–80 kDa. The hutch is connected to an axial channel, which traverses the center of the CED-4 apoptosome and measures 60 Å in length and 16–36 Å in diameters. The interior surface of the CED-4 apoptosome is enriched by positively charged amino acids, whereas the exterior exhibits a mixture of acidic and basic electrostatic potential (Figure S1D).

In each CED-4 molecule, the five sequential domains, CARD, α/β-fold, HD1, WHD, and HD2, are arranged approximately in a linear fashion from the narrow end to the wide end of the funnel-shaped complex (Figure 1B). The primary oligomerization interface is mediated by the α/β-fold, HD1, and WHD domains. The CARDs, especially the four at the narrow end of the complex, have high temperature factors, suggesting certain degrees of flexibility (Figure 1C).

Organization of the Three-Layer Ring Structure

The funnel-shaped CED-4 apoptosome is organized into three layers of ring structure (Figure 2). The top, middle, and bottom layers are formed by the CARDs, the α/β-fold and HD1, and the HD1 and WHD, respectively. The top layer consists of eight CARDs, which are arranged in two contrasting orientations (Figure 2A). Four CARDs form a symmetric tetramer, capping the narrow end of the funnel (Figure 2A, colored green). These four CARDs make no direct interactions with the α/β-fold or the HD1; rather, they interdigitate with four additional CARDs that directly interact with the middle layer. The two different CARD positions relative to the rest of the CED-4 molecules are matched by the different conformations of a 13 residue linker sequence (residues 98–110), which connect the CARD to the α/β-fold (Figure S1F). Together, these eight CARDs form a staggered ring with four-fold symmetry.

In the middle layer, eight α/β domains stack against one another to form a closed ring, with the HD1 domains radiating outwards and making few interactions with adjacent α/β domains (Figure 2B). In the bottom layer, eight HD1 domains alternate with eight WHD domains to form a large ring structure (Figure 2C). Together, the middle and the bottom layers are
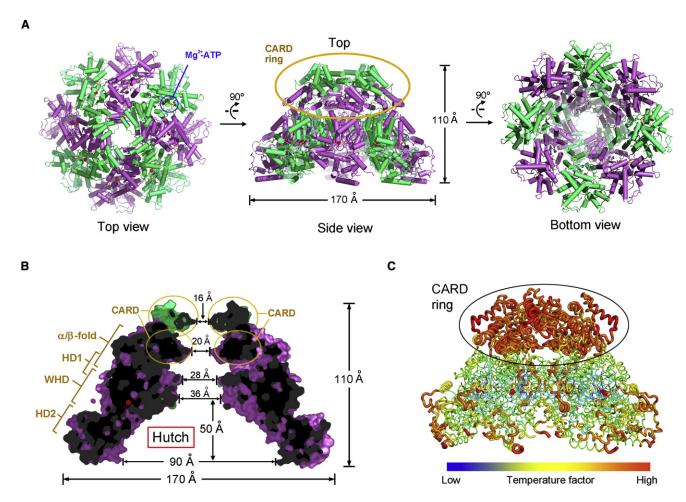
Figure 1. Structure of the CED-4 Apoptosome

(A) Overall structure of the CED-4 apoptosome in three perpendicular views. The CED-4 apoptosome is a tetramer of the asymmetric CED-4 homodimer, with the two CED-4 molecules colored green and magenta. Each CED-4 contains a deeply buried ATP molecule and a Mg^{2+} ion.

(B) A section of the CED-4 apoptosome through the central axis. This representation highlights the hutch—the cone-shaped space within the apoptosome.

(C) The CARDs have high temperature factors. All structural figures were prepared using PyMol (DeLano, 2002).

See also Figure S1.

intertwined, involving a buried surface area of approximately 23188 $Å^2$ for eight CED-4 molecules, and constitute the predominant determinant of CED-4 oligomerization. Although the top layer has a four-fold symmetry (Figure 2A), the middle and bottom layers display an approximate eight-fold symmetry (Figures 2B and 2C), where the intermolecular interface within the same CED-4 asymmetric dimer is nearly identical to that between two CED-4 asymmetric dimers.

The interface organization of the CED-4 apoptosome is different from that of all other known AAA$^+$ proteins (Neuwald et al., 1999), which share a generally conserved domain organization at the oligomeric interface (Diemand and Lupas, 2006). In other AAA$^+$ proteins exemplified by the hexameric NSF (N-Ethylmaleimide sensitive factor) (Lenzen et al., 1998; Yu et al., 1998) and heptameric NtrC1 (Lee et al., 2003), the α/β-fold of one molecule interacts predominantly with the HD1 of the adjacent molecule, and both the α/β-fold and the HD1 domains are located approximately within the plane of the ring structure

(Figure S2). By contrast, the α/β-fold of one CED-4 molecule makes only a few interactions with the HD1 of the adjacent molecule, and the HD1 domain is tilted out of the plane of the ring structure toward the wide end of the funnel-shaped CED-4 apoptosome (Figure S2). This domain organization leaves ample space between two adjacent HD1 domains, where WHD binds. Sequence conservation among NB-ARC proteins suggests that this previously unreported oligomerization interface may be conserved in the Apaf-1 apoptosome, the Dark apoptosome, and perhaps the R proteins.

Interface between Adjacent CED-4 Molecules

The eight CED-4 molecules in the apoptosome display two different interfaces between adjacent CED-4 molecules (Figure 3A). To facilitate presentation, the CED-4 molecule with CARD located at the narrow end of the apoptosome is referred to as CED-4b; the other CED-4 is termed CED-4a. The only marked conformational difference between CED-4a and CED-4b
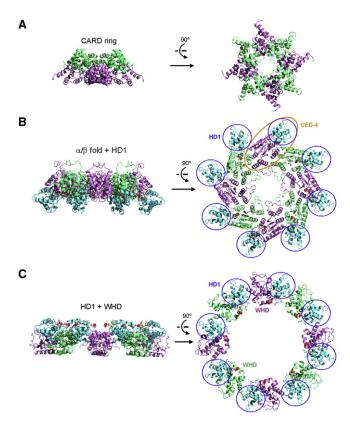
Figure 2. The CED-4 Apoptosome Consists of Three Layers of Stacked Ring Structures

(A) The CARD ring resides at the narrow end of the funnel-shaped CED-4 apoptosome.

(B) The middle ring structure is formed by eight α/β domains (colored green and magenta). The HD1 domains radiate outward and make few interactions with adjacent α/β domains.

(C) The bottom ring structure contains 16 domains, with 8 HD1 domains alternating with 8 WHD domains. The HD1 are colored cyan in all eight subunits, whereas other domains are colored green and magenta to correspond to the two molecules in each asymmetric dimer.

See also Figure S2.

is the location of the CARD relative to the other domains within the same molecule (Figure 3B). In CED-4b, the CARD mainly interacts with two surrounding CARDs from adjacent CED-4a molecules (Figures 3A and 3C). In CED-4a, however, the CARD interacts with four domains: the α/β-fold within the same CED-4a molecule, an α/β-fold from one adjacent CED-4b molecule, and both CARDs from the surrounding CED-4b molecules (Figures 3A and 3C). Interestingly, the CARD from CED-4a maintains the same conformation as that observed in CED-4a from the (CED-4)₂:CED-9 complex (Yan et al., 2005). Given the high temperature factors of the CARDs (Figure 1C), we cannot rule out the possibility that the observed conformation of the CARDs in CED-4b and, to a lesser extent, CED-4a may be influenced by crystal packing.

The principal determinant for formation of the CED-4 apoptosome is the shared interface within the asymmetric CED-4 dimer and between two adjacent CED-4 dimers. This interface involves an extensive buried surface area of 3775 Å² (Figure S3). At this interface, the α/β-fold not only stacks against the HD1 and the

WHD within the same CED-4 molecule but also interacts with the α/β-fold of the adjacent CED-4 molecule.

In *C. elegans*, formation of the CED-4 apoptosome is triggered by EGL-1-mediated release of the asymmetric CED-4 dimer from the (CED-4)₂:CED-9 complex (Yan et al., 2005). Superposition of the (CED-4)₂:CED-9 complex into the CED-4 apoptosome revealed that the structure of the asymmetric CED-4 dimer from the (CED-4)₂:CED-9 complex is nearly identical to that in the CED-4 apoptosome except for the CARD of CED-4b, which was disordered in the (CED-4)₂:CED-9 complex (Figure 3D). Another appreciable difference is the conformation of a loop sequence between helices α11 and α12 in the α/β-fold. The superposition also illustrates that CED-9 from the (CED-4)₂: CED-9 complex overlaps with an adjacent CED-4 molecule in the CED-4 apoptosome, explaining why CED-9 must be displaced in order for the CED-4 apoptosome to assemble.

Implication for the Apaf-1 Apoptosome

Apaf-1 shares approximately 45% sequence similarity with CED-4 in their N-terminal 500 amino acids (Zou et al., 1997) (Figure S4A). Although CED-4 and the autoinhibited Apaf-1 exhibit different overall conformations, the individual domains of CED-4—CARD, α/β-fold, HD1, and WHD—can be superimposed very well with the corresponding domains of Apaf-1 (Figure 4A). For example, the α/β-fold and HD1 domains can be superimposed with a root-mean-square deviation (rmsd) of 1.6 Å for 156 aligned Cα atoms between these two proteins. This analysis suggests that the activated Apaf-1 may have a conformation similar to that of CED-4. A model of the activated Apaf-1 monomer was constructed by placing the CARD, WHD, and HD2 domains into the corresponding positions of CED-4 (Figure 4B).

Next, we generated an atomic model of the Apaf-1 apoptosome using the modeled structure of the activated Apaf-1 (Figure 4C). The seven-fold symmetry was generated by rotating each Apaf-1 molecule by 51.4 (360/7) degrees along a central axis. There is little steric clash among the backbone atoms of the seven Apaf-1 molecules, and the HD2 domains radiate outwards, consistent with the observed features of the electron density map derived from EM studies (Acehan et al., 2002; Yu et al., 2005).

We sought to experimentally corroborate the model of the Apaf-1 apoptosome. In the CED-4 apoptosome, Leu209 on α11 and Leu217/Leu218 in the loop of one CED-4 molecule stack against Val230, Arg233, and Met234 on α12 of an adjacent CED-4 molecule (Figure S4B). Based on the model of the Apaf-1 apoptosome, this part of the intersubunit interface is likely mediated by Asn201/Thr204/Arg205 on α11, Gln208/Arg215 in the intervening loop, and Glu221/Asp225/Arg226 on α12 (Figure S4B). We generated and purified two mutant Apaf-1ΔC proteins (residues 1–591), N201A/T204R/R205E/Q208A (named mut1) and R215D/E221R/D225R/R226D (mut2), and examined their ability to form a miniapoptosome. Although the wild-type (WT) Apaf-1ΔC formed a stable miniapoptosome in the presence of dATP (Riedl et al., 2005), both mutants failed to do so (Figure 4D). To pinpoint the functionally important amino acids, we generated and purified six mutant Apaf-1ΔC proteins, each with a single missense mutation. Although T204R and
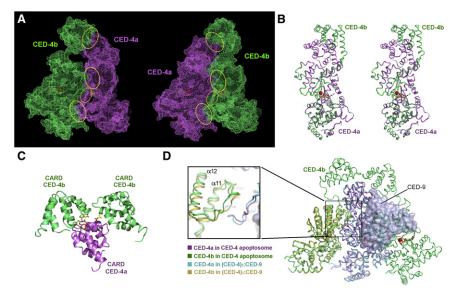
Figure 3. Asymmetry in the CED-4 Apoptosome

(A) The interface from CED-4a to CED-4b is nearly identical to that from CED-4b to CED-4a except for the CARD-CARD interactions. CED-4 is shown in a surface, mesh representation.

(B) A stereo comparison between CED-4a and CED-4b. The only major difference between these two CED-4 molecules is the relative positions of the CARDs.

(C) A close-up view of the CARD-CARD packing interactions.

(D) Superposition of the (CED-4)$_2$:CED-9 complex onto the CED-4 apoptosome revealed serious overlap between CED-9 and adjacent CED-4 subunits. This analysis explains why CED-9 must be removed for the CED-4 dimer to oligomerize. See also Figure S3.

Q208A behaved similarly to the WT protein, four Apaf-1ΔC mutants—N201A, E221R, D225R, and R226D—crippled the ability to form a miniapoptosome (Figure 4E).

Our structure-based model differs from the published model of the Apaf-1 apoptosome (Figure 4F). There are three major differences. First, in our model, the α/β-fold of one Apaf-1 molecule directly interacts with the α/β-folds of neighboring Apaf-1 molecules. In the published model (Acehan et al., 2002; Yu et al., 2005), however, there is no direct contact between these domains. Second, in our model, the CARDs are positioned above the main ring structure, away from the central axis, and do not make major contributions to apoptosome formation
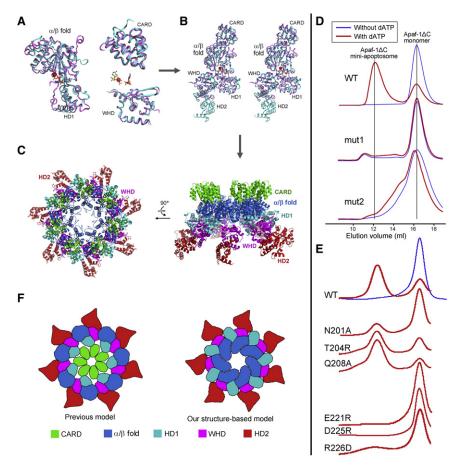
Figure 4. Assembly of the Apaf-1 Apoptosome

(A) Individual domains of CED-4 and Apaf-1 are structurally conserved. This comparison gives rise to the basis for where interdomain movement should occur in Apaf-1 in response to ATP/dATP binding.
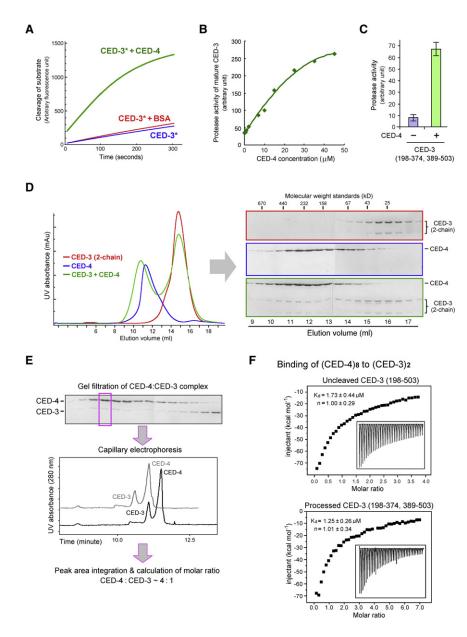
(B) Superposition of CED-4 (magenta) and the modeled, activated Apaf-1 (cyan).

(C) An atomic model of the Apaf-1 apoptosome on the basis of the CED-4 apoptosome. Note that the CARDs do not make a major contribution to ring formation in this model.

(D) Mutation of residues at the predicted interface of the Apaf-1 apoptosome resulted in abrogation of apoptosome formation. Shown here are chromatograms of gel filtration. Two mutants of Apaf-1ΔC, one containing N201A/T204R/R205E/Q208A (mut1) and the other R215D/E221R/D225R/R226D (mut2), both led to loss of apoptosome assembly.

(E) Identification of individual amino acids that contribute to the formation of the Apaf-1 apoptosome. Six mutant Apaf-1ΔC proteins, each with a single missense mutation, were generated and evaluated for their ability to form a miniapoptosome.

(F) Our structure-based model of the Apaf-1 apoptosome differs from the published model (Acehan et al., 2002; Yu et al., 2005). See also Figure S4.

A

CED-3* + CED-4

CED-3* + BSA

CED-3*

B

C

CED-3
(198-374, 389-503)

D

Molecular weight standards (kD)

CED-3 (2-chain)
CED-4
CED-3 + CED-4

CED-3
(2-chain)

CED-4

CED-4

CED-3
(2-chain)

E

Gel filtration of CED-4:CED-3 complex

CED-4
CED-3

Capillary electrophoresis

CED-4

CED-4

CED-3

CED-3

Peak area integration & calculation of molar ratio
CED-4 : CED-3 ~ 4 : 1

F

Binding of (CED-4)₈ to (CED-3)₂

Uncleaved CED-3 (198-503)

$K_d = 1.73 \pm 0.44 \mu M$
$n = 1.00 \pm 0.29$

Processed CED-3 (198-374, 389-503)

$K_d = 1.25 \pm 0.26 \mu M$
$n = 1.01 \pm 0.34$

Figure 5. CED-4 and Processed CED-3 Form a Stable Holoenzyme

(A) The processed CED-3 exhibited higher levels of protease activity in the presence of CED-4. Shown here is a representative result of four independent experiments.

(B) The protease activity of processed CED-3 was stimulated by CED-4 in a concentration-dependent manner. Shown here is a representative result of three independent experiments.

(C) CED-4 stimulated the protease activity of the two-chain CED-3 (residues 198–374, 389–503, D221A). The error bars represent standard deviations of ten independent experiments.

(D) The CED-4 apoptosome formed a stable complex with the two-chain CED-3 (residues 198–374, 389–503, C358A). Shown on the left are representative gel-filtration chromatograms of CED-4 alone, CED-3, and CED-4 incubated with excess CED-3. The peak fractions were visualized on SDS-PAGE.

(E) The CED-4 apoptosome also formed a stable complex with the CED-3 zymogen (residues 198–503, C358A). The peak fraction of the CED-4:CED-3 complex from gel filtration was subjected to capillary electrophoresis under denaturing conditions. Shown here is a representative result of five independent experiments. This analysis yielded a calculated molar ratio of 3.8 ± 0.2 for CED-4 over CED-3. The error bar represents standard error of the mean.

(F) Quantitative analysis of the CED-4:CED-3 interactions confirmed the 4:1 molar ratio. Binding of uncleaved CED-3 (residues 198–503, C358A) or two-chain CED-3 (residues 198–374, 389–503, C358A) by CED-4 was examined by isothermal titration calorimetry (ITC).

See also Figure S5.

CED-4 can also stimulate the protease activity of the processed CED-3. To examine this scenario, we attempted to express and purify recombinant CED-3 protein. We expressed the WT, full-length CED-3 and a number of mutant CED-3 proteins in *E. coli*, *Saccharomyces cerevisiae*, or baculovirus-infected insect cells. Despite overexpression, the full-length CED-3 proteins were insoluble. We were able to solubilize the full-length CED-3 by in vitro refolding; however, the refolded CED-3 protein was prone to aggregation and unfit for biochemical characterization. After testing dozens of constructs, we found a 34 kDa CED-3 fragment (residues 198–503) that exhibited good solution behavior, allowing enzymatic and biophysical investigation. Expression of this CED-3 fragment in *E. coli* gave rise to fully processed, active CED-3 protease (Figure S5A); whereas mutation of the catalytic residue Cys358 to Ser allowed purification of this fragment to homogeneity (Figure S5B).

We investigated the impact of CED-4 on the protease activity of the processed, active CED-3 using the fluorogenic substrate DEVD-AMC (Figure 5A). The processed CED-3 exhibited a basal

(Figure 4C). By contrast, the published model placed the CARDs in a closed ring structure around the central axis, which appears to contribute to apoptosome formation (Figure 4F). Third, the WHD domains are thought to bridge adjacent HD1 domains in our model, whereas they were proposed to link adjacent, noninteracting α/β domains in the EM-based model. A modeling study suggested that the published model of the Apaf-1 apoptosome may conflict with a number of structural considerations (Diemand and Lupas, 2006).

CED-4 Markedly Stimulates the Protease Activity of Processed CED-3

The CED-4 apoptosome facilitates the autocatalytic processing of the CED-3 zymogen (Seshagiri and Miller, 1997; Yan et al., 2005; Yang et al., 1998b). It is unclear, however, whether

level of protease activity. Incubation of CED-3 with the full-length, WT CED-4 led to a markedly enhanced level of protease activity. This effect is specific to CED-4, as incubation with BSA failed to enhance the protease activity. Importantly, the increase of the CED-3 protease activity is correlated with increasing concentrations of CED-4, suggesting saturable interactions between CED-4 and the processed CED-3 protease (Figure 5B). In these experiments, the processed, active CED-3 protease was derived from the 34 kDa CED-3 fragment (residues 198–503), which was autocatalytically processed during overexpression in *E. coli*. Similar results were obtained for a two-chain CED-3 protease (residues 198–374 and 389–503) (Figure 5C), which was generated by coexpression of the two chains in *E. coli*. These observations demonstrate that, under the experimental conditions tested, the CED-4 apoptosome stimulated the protease activity of the mature CED-3 protease by 5- to 10-fold.

Formation of a CED-3-CED-4 Holoenzyme

Stimulation of CED-3 activity by CED-4 suggests that the processed CED-3 protease may form a stable complex with the CED-4 apoptosome. We generated a two-chain CED-3 variant (residues 198–374 and 389–503, C358S) and examined its potential interaction with CED-4 using gel filtration. Mutation of the catalytic residue Cys358 to Ser was essential to allow accumulation of sufficient CED-3 protein for biochemical characterization. The elution volume for the two-chain CED-3 alone from gel filtration corresponded to a molecular mass of ∼35 kDa (Figure 5D), consistent with that of a monomer. Upon incubation with CED-4, a portion of the two-chain CED-3 was shifted to earlier fractions and was coeluted with the CED-4 apoptosome. These observations indicate that the two-chain CED-3 (C358S) formed a stable complex with the CED-4 apoptosome. Curiously, however, the molar ratio between CED-4 and CED-3, as suggested by the intensity of Coomassie blue staining (Figure 5D), did not appear to be 1:1. Similar to the two-chain CED-3, the unprocessed, single-chain CED-3 (residues 198–503, C358S) also formed a stable complex with the CED-4 apoptosome (Figure 5E). In both cases, the molar quantity of CED-3 seemed to be substantially less than that of CED-4.

To determine the molar ratio between CED-4 and CED-3, we applied the preassembled, stoichiometric CED-4-CED-3 complex to capillary electrophoresis under denaturing conditions, which separated CED-3 from CED-4 (Figure 5E). The proteins were detected by UV absorbance at 280 nm, and the total UV absorbance for CED-3 and CED-4 was integrated. The total molar quantities of CED-3 and CED-4 were derived by dividing their total UV absorbance by their respective molar extinction coefficients at 280 nm. This analysis, representing five independent experiments, yielded a calculated molar ratio of 3.8 ± 0.2 for CED-4 over CED-3. Consistent with this analysis, quantification of gel-filtration experiments yielded a molar ratio of approximately 4:1 between CED-4 and CED-3. These observations suggest that the octameric CED-4 complex may associate with only two, rather than eight, molecules of CED-3.

To further characterize the interactions, we determined the binding affinity between CED-3 and CED-4 using isothermal titration calorimetry (ITC). The concentrations of CED-4 octamer and CED-3 dimer were used to fit the binding curves (Figure 5F).

The CED-4 apoptosome bound to the uncleaved CED-3 (residues 198–503, C358S) and the two-chain CED-3 (residues 198–374, 389–503, C358S) with dissociation constants of approximately 1.73 ± 0.44 μM and 1.25 ± 0.26 μM, respectively. In both cases, the molar ratio between the CED-4 octamer and the CED-3 dimer was fitted to be approximately 1.0, confirming the notion that the CED-4 apoptosome may only associate with two molecules of CED-3.

Model of the CED-4:CED3 Complex

For all known caspases, the active form is a homodimer because formation of the active site in one protomer requires the L2′ loop from the adjacent protomer through loop-bundle interactions (Shi, 2002). We suspected that the CED-4 apoptosome may help assemble a CED-3 homodimer, thus stimulating its protease activity. In this case, free CED-3 was speculated to exist as a monomer in solution. Supporting this notion, both the uncleaved CED-3 fragment (residues 198–503, C358S) and the two-chain CED-3 (residues 198–374, 389–503, C358S) were eluted from gel filtration with an apparent molecular mass of ∼35 kDa, consistent with that of a monomer (Figure S5C). This observation suggests that the intrasubunit cleavage failed to induce dimerization of CED-3. This result is reminiscent of the mammalian initiator caspase-9 (Shiozaki et al., 2003) and contrasts the scenario for caspase-8 (Boatright et al., 2003; Donepudi et al., 2003) or the *Drosophila* initiator caspase Dronc (Yan et al., 2006a). Supporting this finding, sedimentation equilibrium analysis of the two-chain CED-3 revealed a molecular weight of 35.25 kDa (Figure S5D), similar to the calculated molecular weight of 34.29 kDa for the monomeric CED-3 (residues 198–503, C358S).

Our experimental observations suggest a scenario in which the octameric CED-4 apoptosome associates with two monomers of CED-3 and mediates their activation. To gain insights into this process, we crystallized a stable complex between the CED-4 apoptosome and the two-chain CED-3 or the uncleaved CED-3 (residues 198–503, C358S) in the space group I422. Analysis of the crystals by SDS-PAGE revealed the presence of both CED-4 and CED-3, with the intensities of Coomassie staining consistent with the 8:2 molar ratio between CED-4 and CED-3 (Figure 6A, inset; Figure S6A). The structure was refined at 3.9 Å resolution (Table S2). Despite the presence of CED-3 in the crystals, there was no discernable electron density for CED-3. This unanticipated outcome can be explained by CED-4 packing in the crystals. Each asymmetric unit contains two protomers of CED-4, and the octameric CED-4 complex is formed via a four-fold crystallographic symmetry operation. Examination of the crystal lattice indicated that there are only two potential locations that are large enough to accommodate two protomers of CED-3. One is outside the CED-4 octamer, between four pairs of CED-4 protomer, with each pair coming from a distinct CED-4 apoptosome (Figure S6B). This arrangement would give rise to a molar ratio of 1:1 between CED-4 and CED-3, inconsistent with experimental observations. The only other location is the hutch of the funnel-shaped CED-4 octamer (Figure 5A). In this case, the electron density for CED-3 may be averaged to noise level due to at least four potential binding orientations in the hutch.
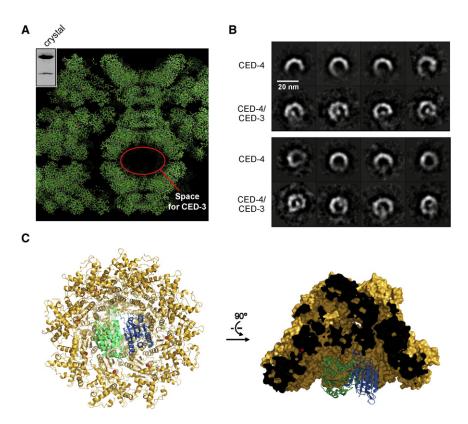
Figure 6. The CED-4 Apoptosome May Bind to the Processed CED-3 within the Hutch

(A) Structure of the CED-4:CED-3 complex. Despite presence of the CED-3 protein in the crystals, there was no apparent electron density for it. The hutch of the CED-4 apoptosome in the crystal is large enough to accommodate the CED-3 dimer. This scenario also provides a plausible explanation as to why there was no electron density for CED-3, as the four-fold crystallographic symmetry operator likely decimated the electron density for CED-3 that could bind in multiple orientations within the hutch of the CED-4 octamer.

(B) Cryo-EM analysis of the complex between CED-4 and two-chain CED-3. Examination of the averaged cryo-EM images of the complex between CED-4 and two-chain CED-3 revealed some electron density in the center of the CED-4 apoptosome. This density, indicative of CED-3, is absent in the averaged cryo-EM images of the CED-4 apoptosome alone. Shown here are the side views of the CED-4 particle and the CED-4:CED-3 complex.

(C) A model of the CED-4 apoptosome bound to the catalytic core domain of CED-3 dimer.

See also Figure S6.

Although the multiple, contrasting orientations of CED-3 within the CED-4 apoptosome pose a problem for X-ray diffraction, they are amenable to cryo-EM analysis. In agreement with the above analysis, cryo-EM investigation of the CED-4:CED-3 complex revealed extra electron density within the CED-4 apoptosome (Figure 6B). The size and location of these extra densities are consistent with those predicted for CED-3. In addition, the size of the CED-4 particles is consistent with the crystal structure of the CED-4 apoptosome. Importantly, these extra electron densities are absent in the averaged images of the CED-4 apoptosome alone. These observations suggest that two molecules of CED-3 may be accommodated in the hutch (Figure 6C).

DISCUSSION

The CED-4 Apoptosome Is a Tetramer of Dimers

Our previous EM study suggested a four-fold symmetry within the CED-4 apoptosome, which was interpreted as a tetramer of the CED-4 molecule (Yan et al., 2005). However, fitting four molecules of CED-4 into the EM density invariably left a substantial portion of the density unaccounted for. In addition, our biochemical data strongly suggested that the interface in the CED-4 apoptosome is very similar to that between two molecules within the same asymmetric CED-4 dimer (Yan et al., 2005). If the interface between the asymmetric CED-4 dimer were to be propagated, the resulting, closed CED-4 ring would involve eight, not four, molecules. Our current structure provides a satisfactory solution to these problems. Due to the contrasting CARD conformations, the CED-4 apoptosome exhibits a perfect four-fold symmetry, consistent with previous EM observations

(Yan et al., 2005). However, the basic structural unit is an asymmetric dimer of CED-4, not a monomer. The eight molecules of CED-4 nicely occupy the electron density in the EM-based map of the CED-4 apoptosome.

Activation of the NB-ARC Proteins

The R proteins constitute a central component of the plant immune system (Belkhadir et al., 2004; Takken et al., 2006). In response to a pathogen avirulence gene product (AVR), the R protein is activated and triggers a host defense response. In animals, the nucleotide-binding, oligomerization (NOD)-like receptors (NLRs) are intracellular sensors of microbial pathogens and other signals (Petrilli et al., 2007). NLRs are essential components of the animal immune and inflammation responses. Most R proteins and NLRs belong to the NB-ARC family. Each NB-ARC protein contains an N-terminal signaling domain (typically a CARD, a pyrin, or a coiled-coil (CC)/Toll and Interleukin 1 receptor (TIR) domain), a nucleotide-binding domain (α/β-fold and HD1), a WHD, and a C-terminal protein-protein interaction motif, usually WD40 or LRR repeats (Figure S4A).

The NB-ARC proteins exist in an inactive state prior to signaling. CED-4 is maintained in an inactive state through CED-9 sequestration (Chen et al., 2000; James et al., 1997; Spector et al., 1997; Wu et al., 1997; Yan et al., 2005). Structural analysis revealed that Apaf-1 exists in an autoinhibited state through binding to ADP and through extensive intradomain interactions (Riedl et al., 2005). Both CED-4 and Apaf-1 must undergo an activation process to form the death-inducing apoptosomes (Figure 7). In the case of CED-4, the upstream protein EGL-1 is needed to disrupt the CED-4-CED-9 interaction and to release
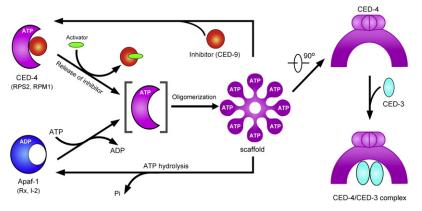
CED-4 from the inhibitory complex (Conradt and Horvitz, 1998; del Peso et al., 1998; Yan et al., 2004). The freed CED-4 dimer further tetramerizes to form the CED-4 apoptosome. In the case of Apaf-1, upstream cell death signaling causes the release of cytochrome *c* from mitochondria, which binds to Apaf-1 and allows Apaf-1 to exchange ADP/dADP for ATP/dATP (Bao et al., 2007; Kim et al., 2005; Li et al., 1997). The binding of ATP/dATP is the decisive event that leads to the formation of the mammalian apoptosome.

How do other NB-ARC proteins maintain their inactive states? Although a definitive answer is still at large, biochemical and structural studies of CED-4 and Apaf-1 offer tantalizing clues. We hypothesize that some NB-ARC proteins, such as the R proteins RPS2 and RPM1, may emulate CED-4 and attain their default, inactive states through interaction with other partner proteins, such as RIN4 (Axtell and Staskawicz, 2003; Mackey et al., 2002, 2003) (Figure 7). Other NB-ARC proteins, such as the potato protein Rx (Moffett et al., 2002) and the tomato protein I-2, are likely to be similar to Apaf-1 and maintain their dormancy through intramolecular interactions (Figure 7).

Upon activation, the NB-ARC proteins are thought to form an oligomeric complex. The shared sequence and domain homology among the NB-ARC proteins suggests common principles for assembly of the activated complex. In analogy to CED-4, other NB-ARC proteins, such as Apaf-1 (Figure 4) and the tobacco N disease resistance protein (Mestre and Baulcombe, 2006), are predicted to assemble into an activated complex via domain organizations similar to those observed in the CED-4 apoptosome. Specifically, the WHD domain in each of these NB-ARC proteins likely plays an essential role in oligomerization, cushioning interdomain interactions and moderating ATP binding and hydrolysis.

Implication for CED-3 Activation

Previous investigations showed that CED-4 facilitates the autocatalytic processing of the CED-3 zymogen (Seshagiri and Miller, 1997; Yan et al., 2005; Yang et al., 1998b). Our current studies demonstrate that the processed CED-3 protease forms a stable holoenzyme with the CED-4 apoptosome, within which CED-3 exhibits enhanced protease activity. This case is similar to that of the caspase-9:Apaf-1 holoenzyme (Rodriguez and Lazebnik, 1999). Both CED-3 and caspase-9 exist as a monomer in their zymogen forms, and both proteins continue to be monomeric

after their autocatalytic cleavages. In both cases, the processed caspase physically associates with the apoptosome to form an active holoenzyme, within which the protease activity of the caspase is markedly stimulated. These similarities suggest that the principles derived from this study may be relevant for understanding caspase-9 activation.

One unanticipated finding is that the molar ratio between CED-4 and processed CED-3 is far from 1:1 in the CED-4:CED-3 complex. Our observation is consistent with the study by Bratton and colleagues (Malladi et al., 2009), where caspase-9 was found to be present at a significantly lower molar quantity compared to Apaf-1 in the caspase-9:Apaf-1 holoenzyme. Experimental evidence from our own laboratory supports this finding (data not shown). Although the precise molar ratio remains to be determined, the Apaf-1 apoptosome appears to only recruit two to four, but not seven, molecules of caspase-9. This scenario contrasts the prevailing model of caspase-9 activation (Boatright and Salvesen, 2003; Pop et al., 2006), which predicted that the Apaf-1 apoptosome recruited seven molecules of caspase-9 and the sheer proximity of these caspase-9 molecules drove their dimerization and subsequent activation.

The CARD of Apaf-1 was previously shown to be responsible for the recruitment of caspase-9 through a CARD-CARD interaction of 1:1 molar ratio (Li et al., 1997; Qin et al., 1999). Why can't the Apaf-1 apoptosome recruit seven molecules of caspase-9 then? One possibility is that binding of caspase-9 CARD to an Apaf-1 molecule may create steric hindrance for neighboring Apaf-1 molecules, preventing their interaction with additional caspase-9 molecules. Another possibility is that association of a caspase-9 molecule to the apoptosome may induce local conformational rearrangements that impose a limit on recruitment of additional caspase-9 molecules. A precise answer to this question remains to be investigated.

The fact that only two molecules of CED-3 may be recruited by the CED-4 apoptosome strongly suggests that these two molecules of CED-3 may be activated through CED-4-assisted homodimerization. The hutch of the CED-4 apoptosome seems to be ideally designed to facilitate the docking and dimerization of two CED-3 molecules—it may drastically increase the chance for two CED-3 molecules to dimerize with each other and at the same time decrease the likelihood of dissociation for the assembled CED-3 homodimer. In this regard, the mechanism of CED-3 activation is best represented by the Induced Conformation model (Chao et al., 2005; Shi, 2004). This mechanism is somewhat analogous to the protein folding chamber of GroEL—unfolded substrate protein is trapped inside for efficient refolding (Horwich et al., 2006). The volume of the hutch in the CED-4

apoptosome is ~150,000 Å^3, compared to a cavity volume of ~120,000 Å^3 in GroES-bound GroEL (Horwich et al., 2006).

The protease activity of caspase-9 is stimulated by 2–3 orders of magnitude by the Apaf-1 holoenzyme (Rodriguez and Lazebnik, 1999; Saleh et al., 1999; Zou et al., 1999). By contrast, the CED-4 apoptosome can only stimulate the protease activity of processed CED-3 by 5- to 10-fold. Why is there such a large difference? This could be explained by differences in substrate-induced dimerization. In the case of caspase-9, binding to covalent inhibitors had little impact on its monomeric state (Shiozaki et al., 2003). By contrast, incubation of the processed CED-3 with DEVD-CHO shifted a portion of CED-3 from monomer to dimer, as judged by gel filtration (Figure S6C). Thus, compared to caspase-9, the processed CED-3 is much more likely to undergo homodimerization in the presence of substrate, giving rise to a higher basal level of protease activity. Consequently, presence of the apoptosome, which serves to facilitate homodimerization of the caspase, had stronger impact on caspase-9 than on CED-3.

EXPERIMENTAL PROCEDURES

Protein Preparation and Assembly of the CED-4 Apoptosome
All constructs and point mutations were generated using a standard PCR-based cloning strategy. The (CED-4)$_2$:CED-9 complex and GST-EGL-1 were purified to homogeneity as described (Yan et al., 2004, 2005). The homogeneous CED-4 apoptosome was obtained as described (Yan et al., 2005). Wild-type and mutant human Apaf-1ΔC (residues 1–591) proteins were purified as described (Riedl et al., 2005). All clones of CED-3, with a C-terminal His$_6$ tag, were expressed or coexpressed in *E. coli* BL21(DE3). Soluble protein was purified using Ni-NTA affinity resin, followed by gel filtration (Superdex-200). An excess amount of the purified CED-3 protein was incubated with CED-4 at 4°C for 30 min. The stable CED-4:CED-3 complex was further purified by gel filtration.

Structure Determination of the CED-4 Apoptosome
All crystals were grown at 18°C. Fresh crystals were transferred into a cryoprotectant buffer containing 20% glycerol and flash-frozen in liquid nitrogen for data collection. Native datasets were collected from single crystals at the SSRF BL17U beamline and processed with HKL2000 (Otwinowski and Minor, 1997). The crystals belong to the space group I422, with a = b = 181.6 Å, c = 203.2 Å. The structure was determined by molecular replacement using Phaser (McCoy et al., 2005). After cycles of rigid body and restraint refinements by Refmac (Murshudov et al., 1999), the linker region (residues 91–108) of CED-4b was manually built in O (Jones et al., 1991). ATP and Mg^{2+} were modeled in the same way as they are in the (CED-4)$_2$:CED-9 complex (Yan et al., 2005). Subsequent refinements of coordinates, individual B factors, and TLS groups were done in phenix.refine (Adams et al., 2002). NCS restraints were maintained throughout refinement.

Modeling Apaf-1 Heptamer
The atomic coordinates of individual domains of Apaf-1 (Protein Data Bank code 1Z6T) were superimposed with the corresponding domains of CED-4a in O (Jones et al., 1991). The new PDB files were combined to generate an Apaf-1 monomer in extended conformation. The Apaf-1 heptamer model was then generated by rotating the modified monomer along a central rotation axis, at a step of ~51.4°, seven times successively with CCP4 program PDBSET (Collaborative Computational Project, 1994).

Mutagenesis Analysis of the Apaf-1 Miniapoptosome
For assembly of the Apaf-1 miniapoptosome, wild-type and mutant Apaf-1 (residues 1–591) were incubated with 1 mM dATP at 4°C for 4 hr as described (Bao et al., 2007).

Structure Determination of the CED-4:CED-3 Complex
The crystals belong to space group I422, with a = b = 181.33 Å, c = 202.88 Å, α = β = γ = 90°. Data were collected at the Spring-8 beamline BL41XU and processed with the HKL2000 package (Otwinowski and Minor, 1997). The atomic coordinates of CED-4 from the PDB entry 2A5Y (Yan et al., 2005) were used for molecular replacement with the program PHASER (McCoy et al., 2005). Manual model building was done using the program COOT (Emsley and Cowtan, 2004). The model was refined in the program PHENIX (Adams et al., 2002).

Electron Microscopy
The frozen-hydrated samples were imaged at a JEOL 2010F electron microscope operating at 200 kV. Images were recorded on Kodak SO-163 negative films, and the films were developed in the full-strength Kodak D-19 developer. The single particle images, 27704 and 21549 for CED-4 and CED-4-CED-3, respectively, were classified and averaged in EMAN (Ludtke et al., 1999).

In Vitro Translation of CED-3
The experiments were performed as described (Yan et al., 2005).

Capillary Electrophoresis
The denatured proteins were separated by capillary electrophoresis and detected at 280 nm by a UV spectrophotometer. A 31.2 cm × 75 μm, uncoated fused-silica capillary was used and the separation voltage was applied at 3 kV.

Isothermal Titration Calorimetry
The unprocessed CED-3 or the two-chain CED-3 was titrated by CED-4. All experiments were performed with a VP-ITC microcalorimeter (MicroCal). The data were fitted using the software Origin 7.0 (MicroCal).

Caspase Assay for CED-3
The fluorogenic peptide Ac-DEVD-AMC was used as the substrate to measure the protease activity of CED-3 variants.

ACCESSION NUMBERS

The atomic coordinates of the CED-4 apoptosome and the CED-3:CED-4 complex have been deposited in the Protein Data Bank with the accession codes 3LQQ and 3LQR, respectively.

SUPPLEMENTAL INFORMATION

Supplemental Information includes Extended Experimental Procedures, six figures, and two tables and can be found with this article online at doi:10.1016/j.cell.2010.03.017.

REFERENCES

Acehan, D., Jiang, X., Morgan, D.G., Heuser, J.E., Wang, X., and Akey, C.W. (2002). Three-dimensional structure of the apoptosome: implications for assembly, procaspase-9 binding, and activation. Mol. Cell *9*, 423–432.

Adams, P.D., Grosse-Kunstleve, R.W., Hung, L.W., Ioerger, T.R., McCoy, A.J., Moriarty, N.W., Read, R.J., Sacchettini, J.C., Sauter, N.K., and Terwilliger, T.C. (2002). PHENIX: building new software for automated crystallographic structure determination. Acta Crystallogr. 58, 1948–1954.

Axtell, M.J., and Staskawicz, B.J. (2003). Initiation of RPS2-specified disease resistance in *Arabidopsis* is coupled to the AvrRpt2-directed elimination of RIN4. Cell 112, 369–377.

Bao, Q., Lu, W., Rabinowitz, J.D., and Shi, Y. (2007). Calcium blocks formation of apoptosome by preventing nucleotide exchange in Apaf-1. Mol. Cell 25, 181–192.

Bao, Q., and Shi, Y. (2007). Apoptosome: a platform for the activation of initiator caspases. Cell Death Differ. 14, 56–65.

Belkhadir, Y., Subramaniam, R., and Dangl, J.L. (2004). Plant disease resistance protein signaling: NBS-LRR proteins and their partners. Curr. Opin. Plant Biol. 7, 391–399.

Boatright, K.M., and Salvesen, G.S. (2003). Mechanisms of caspase activation. Curr. Opin. Cell Biol. 15, 725–731.

Boatright, K.M., Renatus, M., Scott, F.L., Sperandio, S., Shin, H., Pedersen, I.M., Ricci, J.E., Edris, W.A., Sutherlin, D.P., Green, D.R., et al. (2003). A unified model for apical caspase activation. Mol. Cell 11, 529–541.

Chao, Y., Shiozaki, E.N., Srinivasula, S.M., Rigotti, D.J., Fairman, R., and Shi, Y. (2005). Engineering a dimeric caspase-9: a re-evaluation of the induced proximity model for caspase activation. PLoS Biol. 3, e183.

Chen, F., Hersh, B.M., Conradt, B., Zhou, Z., Riemer, D., Gruenbaum, Y., and Horvitz, H.R. (2000). Translocation of C. elegans CED-4 to nuclear membranes during programmed cell death. Science 287, 1485–1489.

Collaborative Computational Project, Number 4 (1994). The CCP4 suite: programs for protein crystallography. Acta Crystallogr. D50, 760–763.

Conradt, B., and Horvitz, H.R. (1998). The *C. elegans* protein EGL-1 is required for programmed cell death and interacts with the Bcl-2-like protein CED-9. Cell 93, 519–529.

Danial, N.N., and Korsmeyer, S.J. (2004). Cell death: Critical control points. Cell 116, 205–219.

del Peso, L., Gonzalez, V.M., and Nunez, G. (1998). Caenorhabditis elegans EGL-1 disrupts the interaction of CED-9 with CED-4 and promotes CED-3 activation. J. Biol. Chem. 273, 33495–33500.

DeLano, W.L. (2002). The PyMOL Molecular Graphics System. on World Wide Web http://www.pymol.org.

Diemand, A.V., and Lupas, A.N. (2006). Modeling AAA+ ring complexes from monomeric structures. J. Struct. Biol. 156, 230–243.

Donepudi, M., Mac Sweeney, A., Briand, C., and Grutter, M.G. (2003). Insights into the regulatory mechanism for caspase-8 activation. Mol. Cell 11, 543–549.

Emsley, P., and Cowtan, K. (2004). Coot: model-building tools for molecular graphics. Acta Crystallogr. 60, 2126–2132.

Horvitz, H.R. (2003). Worms, life, and death (Nobel lecture). ChemBioChem 4, 697–711.

Horwich, A.L., Farr, G.W., and Fenton, W.A. (2006). GroEL-GroES-mediated protein folding. Chem. Rev. 106, 1917–1930.

James, C., Gschmeissner, S., Fraser, A., and Evan, G.I. (1997). CED-4 induces chromatin condensation in *Schizosaccharomyces pombe* and is inhibited by direct physical association with CED-9. Curr. Biol. 7, 246–252.

Jones, T.A., Zou, J.-Y., Cowan, S.W., and Kjeldgaard, M. (1991). Improved methods for building protein models in electron density maps and the location of errors in these models. Acta Crystallogr. A 47, 110–119.

Kanuka, H., Sawamoto, K., Inohara, N., Matsuno, K., Okano, H., and Miura, M. (1999). Control of the cell death pathway by Dapaf-1, a *Drosophila* Apaf-1/ CED-4-related caspase activator. Mol. Cell 4, 757–769.

Kim, H.E., Du, F., Fang, M., and Wang, X. (2005). Formation of apoptosome is initiated by cytochrome c-induced dATP hydrolysis and subsequent nucleotide exchange on Apaf-1. Proc. Natl. Acad. Sci. USA 102, 17545–17550.

Lee, S.Y., De La Torre, A., Yan, D., Kustu, S., Nixon, B.T., and Wemmer, D.E. (2003). Regulation of the transcriptional activator NtrC1: structural studies of the regulatory and AAA+ ATPase domains. Genes Dev. 17, 2552–2563.

Lenzen, C.U., Steinmann, D., Whiteheart, S.W., and Weis, W.I. (1998). Crystal structure of the hexamerization domain of N-ethylmaleimide-sensitive fusion protein. Cell 94, 525–536.

Li, P., Nijhawan, D., Budihardjo, I., Srinivasula, S.M., Ahmad, M., Alnemri, E.S., and Wang, X. (1997). Cytochrome c and dATP-dependent formation of Apaf-1/ caspase-9 complex initiates an apoptotic protease cascade. Cell 91, 479–489.

Ludtke, S.J., Baldwin, P.R., and Chiu, W. (1999). EMAN: semiautomated software for high-resolution single-particle reconstructions. J. Struct. Biol. 128, 82–97.

Lupas, A.N., and Martin, J. (2002). AAA proteins. Curr. Opin. Struct. Biol. 12, 746–753.

Mackey, D., Holt, B.F., 3rd, Wiig, A., and Dangl, J.L. (2002). RIN4 interacts with Pseudomonas syringae type III effector molecules and is required for RPM1-mediated resistance in *Arabidopsis*. Cell 108, 743–754.

Mackey, D., Belkhadir, Y., Alonso, J.M., Ecker, J.R., and Dangl, J.L. (2003). *Arabidopsis* RIN4 is a target of the type III virulence effector AvrRpt2 and modulates RPS2-mediated resistance. Cell 112, 379–389.

Malladi, S., Challa-Malladi, M., Fearnhead, H.O., and Bratton, S.B. (2009). The Apaf-1*procaspase-9 apoptosome complex functions as a proteolytic-based molecular timer. EMBO J. 28, 1916–1925.

Martin, G.B., Bogdanove, A.J., and Sessa, G. (2003). Understanding the functions of plant disease resistance proteins. Annu. Rev. Plant Biol. 54, 23–61.

McCoy, A.J., Grosse-Kunstleve, R.W., Storoni, L.C., and Read, R.J. (2005). Likelihood-enhanced fast translation functions. Acta Crystallogr. D Biol. Crystallogr. 61, 458–464.

Mestre, P., and Baulcombe, D.C. (2006). Elicitor-mediated oligomerization of the tobacco N disease resistance protein. Plant Cell 18, 491–501.

Moffett, P., Farnham, G., Peart, J., and Baulcombe, D.C. (2002). Interaction between domains of a plant NBS-LRR protein in disease resistance-related cell death. EMBO J. 21, 4511–4519.

Murshudov, G.N., Vagin, A.A., Lebedev, A., Wilson, K.S., and Dodson, E.J. (1999). Efficient anisotropic refinement of macromolecular structures using FFT. Acta Crystallogr. 55, 247–255.

Neuwald, A.F., Aravind, L., Spouge, J.L., and Koonin, E.V. (1999). AAA+: A class of chaperone-like ATPases associated with the assembly, operation, and disassembly of protein complexes. Genome Res. 9, 27–43.

Otwinowski, Z., and Minor, W. (1997). Processing of X-ray diffraction data collected in oscillation mode. Methods Enzymol. 276, 307–326.

Petrilli, V., Dostert, C., Muruve, D.A., and Tschopp, J. (2007). The inflammasome: a danger sensing complex triggering innate immunity. Curr. Opin. Immunol. 19, 615–622.

Pop, C., Timmer, J., Sperandio, S., and Salvesen, G.S. (2006). The apoptosome activates caspase-9 by dimerization. Mol. Cell 22, 269–275.

Qin, H., Srinivasula, S.M., Wu, G., Fernandes-Alnemri, T., Alnemri, E.S., and Shi, Y. (1999). Structural basis of procaspase-9 recruitment by the apoptotic protease-activating factor 1. Nature 399, 547–555.

Renatus, M., Stennicke, H.R., Scott, F.L., Liddington, R.C., and Salvesen, G.S. (2001). Dimer formation drives the activation of the cell death protease caspase 9. Proc. Natl. Acad. Sci. USA 98, 14250–14255.

Riedl, S.J., Li, W., Chao, Y., Schwarzenbacher, R., and Shi, Y. (2005). Structure of the apoptotic protease activating factor 1 bound to ADP. Nature 434, 926–933.

Rodriguez, A., Oliver, H., Zou, H., Chen, P., Wang, X., and Abrams, J.M. (1999). Dark is a Drosophila homologue of Apaf-1/CED-4 and functions in an evolutionarily conserved death pathway. Nat. Cell Biol. 1, 272–279.

Rodriguez, J., and Lazebnik, Y. (1999). Caspase-9 and Apaf-1 form an active holoenzyme. Genes Dev. 13, 3179–3184.

Saleh, A., Srinivasula, S.M., Acharya, S., Fishel, R., and Alnemri, E.S. (1999). Cytochrome c and dATP-mediated oligomerization of Apaf-1 is a prerequisite for procaspase-9 activation. J. Biol. Chem. *274*, 17941–17945.

Seshagiri, S., and Miller, L.K. (1997). *Caenorhabditis elegans* CED-4 stimulates CED-3 processing and CED-3-induced apoptosis. Curr. Biol. *7*, 455–460.

Shi, Y. (2002). Mechanisms of caspase activation and inhibition during apoptosis. Mol. Cell *9*, 459–470.

Shi, Y. (2004). Caspase activation: Revisiting the induced proximity model. Cell *117*, 855–858.

Shiozaki, E.N., Chai, J., Rigotti, D.J., Riedl, S.J., Li, P., Srinivasula, S.M., Alnemri, E.S., Fairman, R., and Shi, Y. (2003). Mechanism of XIAP-mediated inhibition of caspase-9. Mol. Cell *11*, 519–527.

Spector, M.S., Desnoyers, S., Hoeppner, D.J., and Hengartner, M.O. (1997). Interaction between the C. elegans cell-death regulators CED-9 and CED-4. Nature *385*, 653–656.

Takken, F.L., Albrecht, M., and Tameling, W.I. (2006). Resistance proteins: molecular switches of plant defence. Curr. Opin. Plant Biol. *9*, 383–390.

van der Biezen, E.A., and Jones, J.D. (1998). The NB-ARC domain: A novel signalling motif shared by plant resistance gene products and regulators of cell death in animals. Curr. Biol. *8*, R226–R227.

van Ooijen, G., Mayr, G., Kasiem, M.M., Albrecht, M., Cornelissen, B.J., and Takken, F.L. (2008). Structure-function analysis of the NB-ARC domain of plant disease resistance proteins. J. Exp. Bot. *59*, 1383–1397.

Wu, D., Wallen, H.D., and Nunez, G. (1997). Interaction and regulation of subcellular localization of CED-4 by CED-9. Science *275*, 1126–1129.

Yan, N., and Shi, Y. (2005). Mechanisms of apoptosis through structural biology. Annu. Rev. Cell Dev. Biol. *21*, 35–56.

Yan, N., Gu, L., Kokel, D., Chai, J., Li, W., Han, A., Chen, L., Xue, D., and Shi, Y. (2004). Structural, biochemical, and functional analyses of CED-9 recognition by the proapoptotic proteins EGL-1 and CED-4. Mol. Cell *15*, 999–1006.

Yan, N., Chai, J., Lee, E.S., Gu, L., Liu, Q., He, J., Wu, J.W., Kokel, D., Li, H., Hao, Q., et al. (2005). Structure of the CED-4-CED-9 complex provides insights into programmed cell death in Caenorhabditis elegans. Nature *437*, 831–837.

Yan, N., Huh, J.R., Schirf, V., Demeler, B., Hay, B.A., and Shi, Y. (2006a). Structure and activation mechanism of the Drosophila initiator caspase Dronc. J. Biol. Chem. *281*, 8667–8674.

Yan, N., Xu, Y., and Shi, Y. (2006b). 2:1 Stoichiometry of the CED-4-CED-9 complex and the tetrameric CED-4: insights into the regulation of CED-3 activation. Cell Cycle *5*, 31–34.

Yang, X., Chang, H.Y., and Baltimore, D. (1998a). Essential role of CED-4 oligomerization in CED-3 activation and apoptosis. Science *281*, 1355–1357.

Yang, X., Chang, H.Y., and Baltimore, D. (1998b). Essential role of CED-4 oligomerization in CED-3 activation and apoptosis. Science *281*, 1355–1357.

Yin, Q., Park, H.H., Chung, J.Y., Lin, S.C., Lo, Y.C., da Graca, L.S., Jiang, X., and Wu, H. (2006). Caspase-9 holoenzyme is a specific and optimal procaspase-3 processing machine. Mol. Cell *22*, 259–268.

Yu, R.C., Hanson, P.I., Jahn, R., and Brunger, A.T. (1998). Structure of the ATP-dependent oligomerization domain of N-ethylmaleimide sensitive factor complexed with ATP. Nat. Struct. Biol. *5*, 803–811.

Yu, X., Acehan, D., Menetret, J.F., Booth, C.R., Ludtke, S.J., Riedl, S.J., Shi, Y., Wang, X., and Akey, C.W. (2005). A structure of the human apoptosome at 12.8 A resolution provides insights into this cell death platform. Structure *13*, 1725–1735.

Yu, X., Wang, L., Acehan, D., Wang, X., and Akey, C.W. (2006). Three-dimensional structure of a double apoptosome formed by the Drosophila Apaf-1 related killer. J. Mol. Biol. *355*, 577–589.

Zhou, L., Song, Z., Tittel, J., and Steller, H. (1999). HAC-1, a *Drosophila* homolog of APAF-1 and CED-4 functions in developmental and radiation-induced apoptosis. Mol. Cell *4*, 745–755.

Zou, H., Henzel, W.J., Liu, X., Lutschg, A., and Wang, X. (1997). Apaf-1, a human protein homologous to *C. elegans* CED-4, participates in cytochrome c-dependent activation of caspase-3. Cell *90*, 405–413.

Zou, H., Li, Y., Liu, X., and Wang, X. (1999). An APAF-1.cytochrome c multimeric complex is a functional apoptosome that activates procaspase-9. J. Biol. Chem. *274*, 11549–11556.